2021-01-15

Graphene oxide biopolymer aerogels for the removal of lead from drinking water using a novel nano-enhanced ion exchange cascade

Bloor, Jonathan

10.1016/j.ecoenv.2020.111422
Ecotoxicology and Environmental Safety
Elsevier

Graphene oxide biopolymer aerogels for the removal of lead from drinking water using a novel nano-enhanced ion exchange cascade

[1]Bloor, J.*, [2]Handy, R. D., [1]Awan, S.A. and [1]Jenkins, D.

[1]School of Engineering, Computing and Mathematics, University of Plymouth, Drake Circus, Plymouth PL4 8AA

[2]School of Biological and Marine Sciences, University of Plymouth, Drake Circus, Plymouth PL4 8AA

*Corresponding author: email, jonathan.bloor@plymouth.ac.uk

Keywords: Aerogel, Graphene oxide, Lead, Potable water, Toxic metals, Filtration.

Abstract

Potable water in developing countries often contains levels of toxic metals that exceed the recommended international limits, with impacts on human health. The aim of the present study was to develop a low cost aerogel synthesised from graphene oxide (GO) cross-linked with alginate to remove Pb^{2+} from potable water. Aerogels were made by a sol-gel of the composite materials followed by a freeze drying method. The shape of the aerogels were 50 mm diameter disks, 5 mm deep and characterised by an open porous network of 50 - 150 micrometres which are mechanically robust upon hydration. Firstly, the study was conducted using a batch adsorption method from a starting concentration 0.48 mM (100mg/l) of Pb^{2+} in ultrapure water over 240 minutes, $n = 4$ with controls. A second series of experiments compared the adsorption of different competing ions at different valencies (Na^{+}, Ca^{2+}, Cu^{2+}, La^{3+}) in an equivalent media. A third series of experiments explored Pb^{2+} desorption from the aerogel at low pH and in highly acidic conditions. This simple filter system, based on a batch adsorption methodology expresses a high affinity for Pb^{2+} resulting in an ultra-high mean maximum adsorption capacity of 504 mg/g of Pb^{2+} within 240 mins at pH 5. The aerogel can also adsorb other toxic metal salts such as La^{3+} and Cu^{2+} with a capacity of 146 and 193 mg/g respectively. Furthermore, the aerogel structure can be acid washed removing 98% of the Pb^{2+} from the structure within three minutes. Overall, the data shows that GO alginate aerogels are highly effective at removing Pb^{2+} from water and the primary mechanism involved is ion exchange, although other phenomenon such as proton tunnelling may be a contributing factor to the ultra-high efficiency of the aerogel for Pb^{2+} remediation.

1. Introduction

Clean potable water is now a global issue that will impact upon nearly 4 billion people by 2030 (Mekonnen and Hoekstra, 2016). With the continued growth of the human population, contamination of potable water from persistent organic pollutants, endocrine disrupting chemicals, pathogens, increasing salinity, organic dyes and toxic metals, as well as ground water shortages are an increasing concern (Di Baldassarre et al., 2018; Talukder et al., 2016). Non-essential metals that are known to bioaccumulate in humans, such as mercury, cadmium, and lead (Pb), are of special concern; as well as metalloids such as arsenic (Sankhla et al., 2016). Of these metals, the removal of Pb from the drinking water and from the infrastructure (i.e., lead piping) has long been implemented in developed countries; with the current maximum allowable total Pb concentration in potable water in the European Union being 10 µg/l (Commission, 1998). The World Health Organisation (WHO) also recommends limits on total Pb in drinking water of 10 µg/l (WHO, 2011). However, due to a lack of infrastructure for water treatment, as well as contamination of soil and groundwater, many developing countries fail to meet the WHO limits. In some cases, Pb concentrations as high as 459 µg/l have been recorded in 'potable' water supplies from boreholes and hand-dug wells (Balli and Leghouchi, 2018).

In humans, respiratory exposure to Pb via dusts or aerosols is usually modest (Boskabady et al., 2018). Some Pb absorption can occur through sweat glands and hair follicles in the skin, but percutaneous absorption through healthy skin is slow, or negligible, depending on the lead salt used (Stauber et al., 1994). Consequently, the main route of uptake in humans is through oral exposure. There is a concern about the incidental ingestion of bioaccessible Pb in soil especially by children (Van de Wiele et al., 2007), and for dietary exposure to contaminated foods such as vegetables (Douay et al., 2013), but contaminated water is a main cause of oral exposure (Edwards, 2013). Pb is absorbed via the small intestine into the blood and bioaccumulates in internal organs, including the liver, kidneys and the central nervous system. Pb is also stored inertly in the skeleton and can be remobilised during pregnancy, causing exposure to the foetus (Lowry, 2010). The major concerns regarding long term Pb exposure include toxicity to the central nervous system, causing intellectual impairment, especially during brain development in children. Lead exposure also effects renal function and has associated cancer risks (Canfield et al., 2003). Clinical monitoring of the human population for Pb exposure usually involves the determination of total Pb concentrations in the blood,

although measuring the hair or fingernails has also been suggested (Barbosa Jr et al., 2005). However, the best way to protect the population is to prevent the exposure.

Conventionally, lead is removed from wastewater by standard sewage treatment processes such as chemical precipitation, flocculation and coagulation (Fu and Wang, 2011). This is cost effective on a large scale and with the ability to remediate relatively high concentrations of metals. Consented discharges from sewage treatment works may contain low µg/L concentrations of Pb, but it may also be desirable to protect any surface or ground water source used for drinking water abstraction. In this regard, adsorption of µg/L concentrations of Pb and other metals can be achieved using activated carbon. Activated carbon can be made from sustainable carbon sources such as rice straw, coconut shell or tree bark; and depending on the surface area of the material, the pH, temperature and ionic strength of the water, it has an adsorption capacity for Pb of around 13-98 mg/g (Wang et al., 2010). However, despite its wide application, activated carbon has some limitation. It is relative expensive to make compared to other natural absorbent materials such as clays, and there are costs associated with the regeneration of the carbon to reactivate it (Zhang, 2002). Nonetheless, in developed countries with good infrastructure, these water treatment methods can provide clean water that meets the current WHO and EU guideline of < 10 µg/l of total Pb in drinking water.

The biggest impacts on health of poor water quality are found in developing countries where the water infrastructure is less reliable, or difficult to implement because much of the population is dispersed in rural areas. The remediation of potable water in remote rural environments often relies upon small water processing stations, and basic filtration techniques using natural materials such as sand, but adsorption remains a most cost-effective mechanisms to remove ‘hidden’ contaminants such as toxic metals (Kundu et al., 2018). There has been considerable research on improving traditional absorbents for metals, including enhancing them with nanomaterials, and alternative materials such as aerogels have also been considered for water treatment (Maleki, 2016).

Aerogels are low density solids with high porosity and ultra-high surface areas offering many advantages as an absorbent including the ability to adsorb a range of metal ions including Pb (Meena et al., 2005), and sometimes at a higher binding capacity than traditional absorbents like clays or activated carbon (Wang et al., 2019). The macroporous nature of aerogel materials provides an open matrix with a high surface area/volume ratio, where the adsorption of metals in solution is not diffusion limited; enabling access to a large number of metal binding sites, a high flux rate, and thus fast sorption kinetics. There is also an opportunity to enhance the performance of aerogels using nanomaterials, and here composite aerogels containing

graphene oxide (GO) have been of particular interest (Zuo et al., 2015). Aerogels made from alginates with added GO can together provide a large number of functional groups; carboxyl ($COOH^-$) and hydroxyl (OH^-) residues, which act as fixed metal binding ligands in the aerogel matrix (Qu et al., 2013). The aerogel structure provides the porosity required for efficient, low cost, point-of-use, toxic metal sorption (Motahari et al., 2016). The standalone alginate or GO aerogels possess weak mechanical strength and structural fragility in comparison with the composite material, but cross-linking of GO and alginates increases the mechanical strength of the overall material and prevents the release of the GO into the environment (Fang and Chen, 2014).

Graphene oxide aerogel composites have been demonstrated for the removal of metal ions such as Cu^{2+} from water (Mi et al., 2012), divalent metals using a GO-MnO_2 composite (Liu et al., 2016), dyes such as methylene blue by an agar-GO composite (Chen et al., 2017a), and even antibiotics using a cellulose-GO composite (Yao et al., 2017). There have been only a few studies that describe Pb^{2+} adsorption by GO and alginate composite aerogels and only in pure water (Pan et al., 2018). However, natural waters show variations in water pH, ionic strength, the presence of water hardness from calcium and magnesium salts; and of course, other trace metals that could be competing ions. Thus, it is important to understand how such aerogels behave in these different conditions of water chemistry. The aim of the present study was to develop a low cost GO and alginate aerogel composite for the removal of Pb^{2+} from water. The specific objectives were to systematically examine the behaviour of the aerogel composite for Pb^{2+} adsorption at different pH values, the effects of ionic strengths, as Na and Ca adsorption, and competing ions in order to understand the utility of the material in different conditions, as well as to quantitatively explore any ion-exchange or other mechanisms involved.

2. Methodology

2.1. Materials

Graphite flakes were purchased from Sigma Aldrich (UK). Supplier's information; purity, 99.8% carbon; the flake size of 50 – 70% of the graphite supplied was 44 µm (325 mesh) or smaller, product code 11349278. Phosphoric acid (85%), sulphuric acid (96 – 98%), hydrogen peroxide (30%), ethanol (absolute), ether (diethyl, anhydrous) and potassium permanganate powder was supplied from Fisher Scientific U.K, all analytical reagent grade.

All ice and water used in the aerogel fabrication and experimental procedures was made from ultrapure water, with a resistivity of 18.2 MΩ at 25 °C. Sodium alginate (CAS number: 9005-38-3), general purpose grade, was supplied from Fisher Scientific. Calcium chloride dehydrate (CAS number: 10035-04-8) and lead (II) nitrate (CAS number: 10099-74-8) powders were supplied from Sigma Aldrich (UK) and used without any modification. All glassware or HDPE vessels used were acid washed and triple rinsed in ultrapure water.

2.2. Graphene Oxide synthesis and characterisation

GO was synthesised using the Improved Hummers Method (IHM) (Marcano et al., 2010). Briefly, graphite was oxidised using strong acids, washed thoroughly and then vacuum dried. The GO production method was completed a minimum of $n = 3$ times with consistent characterisation between each batch. The GO was then characterised using Raman spectroscopy and transmission electron microscopy (TEM) (Figure 1). A stock solution with a total volume of 10 mL at 1% w/v of GO was dispersed in ultrapure water by sonication at 45 kHz for 15 minutes and maintaining a temperature of 4 °C (TRU-SWEEP 575 by Crest Ultrasonics: 120 watts). This dispersion route was used for both Raman and the TEM characterisation (Figure 1). To further prepare the GO specifically for Raman analysis, 5 ml of the stock was pipetted onto an ultrasonically cleaned borosilicate glass slide and left to dry for 48 hr in a vacuum to produce a thin film. The Raman (Horiba XPLORA; laser – 532 nm) measurements were mapped over a 100 micrometre square window on the GO thin film with $n = 20$ mapping points, a 4 x 4 square plus the four outer corners, each 20 micrometres apart. Figure 1A shows the average spectra of all these points confirming the presence of GO, with the expected D-band and G-band peaks. The ratio of the G/D peaks within the GO spectra correspond to the ratio of the Sp^2 hybridised carbon bonds crystalline defects (G-band) and functional groups present (D-band), this value is typically be between 0.8 and 1.2 and is also a good indicator of the oxygen content, the lower the ratio, the less functional groups present (Claramunt et al., 2015).

The TEM analysis (JEOL, JEM-1400) of the GO stock dispersion described above was conducted with 50 µl sub-samples of the dispersion pipetted onto copper TEM grids with a formvar coating, and dried in a vacuum overnight. TEM characterisation using micrographs (Figures 1B - C) resulted in an average platelet size of 3 x 3 to 44 x 44 µm lateral dimensions, measured from a total of $n = 65$ replicate images. The purity of the GO was confirmed by measuring the total metal concentration in the 1% w/v dispersion by inductively coupled

plasma optical emission spectrophotometry (ICP-OES, iCAP 700, Thermo Scientific). Briefly, 1 ml of the stock GO dispersion was digested in 10 ml of *aqua regia* (3:1, HCl : HNO_3) at 90°C for 4 hrs. The trace metal and electrolyte concentrations were all <1 µmol/l (i.e., at or below the detection limit), the presence of potassium (around 4 µmol/l) was also approaching the detection limit (Figure 1D). These observations were consistent with the 99% purity of the graphite source material and confirmed no metal contamination during GO synthesis.

2.3. Aerogel synthesis and characterisation

The aerogel was synthesised by combining sodium alginate and GO into a gel that was then subsequently dried using the simple freeze dry method and further cross-linked using calcium chloride. Alginic acid is a copolymer of α-L-guluronic acid (G block) and β-D-mannuronic acid (M-Block) residues, chemical formula $(C_6H_8O_6)_n$. Sodium alginate $(NaC_6H_7O_6)_n$ is the sodium salt of alginic acid and is formed by the deprotonation of the carboxylic acid (-COOH) group which is replaced by a sodium cation (Figure S1). To prepare the composite, 100 ml of 1% w/v of GO was added to 1.3 l of 2% w/v of sodium alginate at a ratio of 1:13 GO:alginate and mixed using magnetic stirrer until homogeneous. The resulting sol-gel was poured volumetrically into polycarbonate petri dishes and stored at room temperature for 24 h to 'age' the network, the samples were then frozen at -18°C and then transferred to a freeze dryer at -58°C, 450 Torr for 48 hrs. The aerogels were subsequently immersed in 2 l of 4% w/v of calcium chloride ($CaCl_2$) for 16 h to cross-link the G and M acid residues, and then washed in ultrapure water three times to remove excess $CaCl_2$. Finally, the aerogel was re-frozen at -18°C repeating the freeze drying steps, as above. In the presence of the $CaCl_2$ solution, the sodium cations in the alginate are displaced from the -COOH on both mannuronic and guluronic acid residues, resulting in crosslinking of the organic acid residues with the Ca^{2+} cations, forming the calcium alginate $(C_{12}H_{14}CaO_{12})_n$. This process is typically used in the fabrication of alginate based hydrogels (Homayouni et al., 2007). Functional groups on the GO surface, -OH and –COOH, also form ionic bonds with the G and M acid residues of the alginate structure through the Ca^{2+} cations, creating a double network (DN) of crosslinking adding to the mechanical robustness of the aerogel (Figure S1). The resulting aerogels were examined by electron microscopy. Briefly, for SEM analysis the samples were cut whilst submerged in ultrapure water to preserve edges due to blade compression and then dried overnight at ambient temperature in air. The samples were sputter coated with a layer of gold (5 - 10 nm) and scanned using a JEOL, JEM-7001F. Figure 1E illustrates the overall structure

of the aerogel monolith showing the uniformity of pore size and distribution ranging from 50 - 150 µm with a non-specified morphology. Figures 1F and 1G confirmed the average minimum and maximum anisotropic pore sizes found within the structure. Figure 1H shows a high magnification image of a node between adjacent pores within the aerogel, the thickness of the layer is between 5 - 10 µm with an approximate acute angle of 120 degrees between planes.

2.4. Adsorption and desorption methodology

Several series of experiments were conducted. The first explored the adsorption of total Pb from ultrapure water containing Pb as $Pb(NO_3)_2$ at different pH values to inform on the effect of pH-dependent ionisation of the organic residues in the aerogel and/or the effect of H^+ as a competing ion on Pb adsorption. All Nalgene HDPE flasks were acid washed (10% nitric acid) and then triple rinsed in ultrapure water before use. For this experiment, five pH values were selected: pH 3, 4, 5, 7 and 8; and the experiment was conducted in quadruplicate with a control (n = 4 aerogels per treatment in separate flasks). To determine that the Pb^{2+} did not adhere to walls of the vessels, a blank control containing no aerogel was used during each experiment. The experiment conducted at pH 8 resulted in substantial precipitation within the media, and so measured Pb concentrations were excluded from the results. The disappearance of the total Pb from the external media into a 50 mg uniform monolith of aerogel (disc diameter 50 mm, depth 5 mm) was measured over 240 minutes. Briefly, one piece of aerogel was added to 500 ml of 0.48 mM Pb solution in ultrapure water [i.e., 100 mg/L of Pb metal as $Pb(NO_3)_2$] in a HDPE flask and continuously, but gently, stirred at 200 rpm (IKA, RT15) at room temperature, 22 °C. For the Pb treatments at pH 3, 4, 5, and 7, the pH was adjusted by the addition of a few drops of 50 mM of HCl or 0.1M of Trizma® base. The pH was monitored with a glass combination pH electrode and the temperature noted. The aerogel samples remained intact throughout the experiments. At 0, 3, 6, 9, 12, 20, 30, 60, 90, 120 and 240 minutes, 2 ml samples were collected from the solution in each flask, acidified with 80 µl of 6M HNO_3, then subsequently analysed by ICP-OES (iCAP 700, Thermo Scientific) for total Pb concentration. Also, the water samples were subject to a multi-element analysis to determine any ions (e.g., Na^+ and Ca^{2+}) released into the media from the composite aerogel. The experiment at pH 5 was also repeated at 4 °C to determine the effects of temperature on any apparent Pb adsorption.

The second series of experiments explored the effect of competing ions in the external media. In keeping with ion exchange theory, the effects of equimolar concentration of cations

of different valencies (charge densities) was measured in an identical method to the initial Pb experiment above. Sodium (+1), calcium (+2) and lanthanum (+3) were all studied at pH 5, chosen as an optimal pH for dispersion stability, this was done to confirm ion exchange relationship. The metal salt solutions were made from $NaNO_3$, $Ca(NO_3)_2$, lanthanum (III) nitrate hexahydrate $La(NO_3)_3 \cdot 6H_2O$, for sodium, calcium and lanthanum respectively, at an equimolar concentrations of 0.48 mM in ultrapure water with no lead present. Similarly, copper (2+), from copper (II) sulphate pentahydrate $CuSO_{4 \cdot 5}H_2O$, was also studied at pH 5, 0.48 mM, to understand the selectivity of the aerogel, copper has the same valency and a similar charge density to lead and calcium, but unlike calcium, it was not already saturated in the aerogel.

The third series of experiments explored the appearance of Pb from the aerogels into the media. For these desorption experiments, the aerogels were first loaded with approximately 0.1 millimoles absolute of Pb over 240 minutes in an identical procedure to the first series of experiments. Each Pb-loaded aerogel was then transferred to a 500 ml HDPE vessel (acid washed as above) containing ultrapure water, and stirred at room temperature for 240 minutes. Water sample (2 ml) were collected and acidified for metal analysis as above. These desorption experiments were conducted at pH 5 and 3 and the pH of the ultrapure water was adjusted using dropwise additions of HCl at 50 mM, as above. This experiment showed some moderate desorption of Pb from the aerogel and so further experiment was conducted with stronger 2% HCl to try to force an apparent full desorption. In addition, desorption experiments with an oxidising acid, 2% HNO_3 were also performed to determine if degradation of the residues in the gel was possibly responsible for the apparent desorption in the presence of very strong acids. Finally the 50 mg monolith of aerogel was placed in 200 ml of 2% HNO_3 using an HDPE vessel for a 3 month period, shaken by hand once a week, for a qualitative assessment of the mechanical robustness in strong acidic conditions.

2.5. Trace metal analysis

Both the aerogels and the external media were measured for total Pb concentration and/or electrolytes. Briefly, for the aerogels, the 50 mg monolith of the material was removed directly from an adsorption experiment, excess water was gently allowed to drip off each monolith, then added to 10 ml of *aqua regia* (3:1, HCl : HNO_3) and heated to 90°C for 4 hrs, allowed to cool, and then diluted with ultrapure water (18.2 MΩ) and stored in the dark before metal analysis. The digested aerogels and/or the water samples from each experiment were analysed for Pb, Cu, La, Na or Ca as appropriate to the experiment by ICP-OES (iCAP 700,

Thermo Scientific). All samples were analysed against matrix-matched standards and with blanks or standards in the sample run to correct for instrument drift. The limit of detection (LOD) of the ICP-OES for Pb, Cu, La, Na and Ca were, 50, 10, 10, 50 and 50 µg/l respectively.

Further qualitative trace metal analysis was undertaken using Fourier Transform Infrared Spectroscopy (FTIR); Bruker Alpha-P, the IR light source is an ETC EverGlo IR source which has range of 9,600 - 20 cm^{-1}, Potassium Bromide (KBr) beam splitter, range 7,400 - 350 cm^{-1}, detector, denatured triglycine sulphate detector (DTGS), range of 12,500 - 350 cm^{-1}. Briefly, a 50 mg monolith of the aerogel material was removed directly from an adsorption experiment, excess water was gently allowed to drip off each monolith, then clamped to crystal surface after background measurement had been taken, this procedure was completed in triplicate for dry aerogel and for aerogels with and without Pb present.

2.6. Calculations and statistics

The adsorption efficiency (%) of the aerogels for total Pb was calculated using equation (1) and the maximum adsorption capacity (q_e) of the aerogel was calculated using equation (2):

$$\% \, Adsorbed = ((C_0 - C_e)/C_0) \, x \, 100 \quad (1)$$

$$q_e = ((C_0 - C_e) \, x \, V)/m \quad (2)$$

Where; C_o is the initial concentration of the total Pb in (mg/l); C_e is the concentration of the Pb^{2+} at equilibrium in (mg/l); V is the volume of the solution in (l) and m is the weight of the aerogel in (g). All adsorption data are represented as the mean ± SD in mM. Where appropriate, curves were fitted using OriginPro, version 8.6. Where plots were non-linear, curves were fitted using an exponential decay two parameter fit according to the formula:

$$y = A_1.e^{(-x/t1)} + A_2.e^{(-x/t2)} + y_0, \quad (3)$$

where, y_0 = offset, A_1 = amplitude, t_1 = time constant, A_2 = amplitude and t_2 = time constant. Otherwise, linear regressions were used as appropriate to the data. To confirm that plots were statistically different by the end of each experiment, data from the last sample time stamp, as appropriate, were analysed by one way ANOVA followed by Tukey's post-hoc test to locate any differences. Where relevant, the speciation of the total Pb was calculated using Visual

MINTEQ (version 3.1, https://vminteq.lwr.kth.se/download/). The theoretical diffusion rate of the Pb in the media was calculated using the Stokes-Einstein equation (4), this is of particular interest when comparing the diffusion rates at different temperatures:

$$a_H = k_B T / 6\pi\eta D \quad (4)$$

Where; k_B is Boltzman's constant (1.3807 x 10^{-23} J · K $^{-1}$), T is temperature in Kelvin, η is the dynamic viscosity of water (N.s/m^2), D is diffusion coefficient (m^2/s) and a_H is the hydrodynamic radii (nm).

3. Results

Figure 2A shows the apparent adsorption of Pb into the aerogel, as measured by the disappearance of total Pb concentration from the external media (ultrapure water) at pH 3, 4, 5 and 7. The data showed an exponential disappearance of total Pb from the media over time (a two parameter exponential decay, with $r^2 > 0.99$), see Figure 2A. At the end of the experiment, the pH 3 treatment had absorbed significantly less Pb than all the other treatments (ANOVA, $P < 0.05$ and Figure S2). Figure 2B shows the calculated speciation of the Pb in the media with pH, and it is apparent that between pH 3 - 5, the Pb^{2+} ion dominates. At these pH values, and in keeping with the competitive adsorption of Pb^{2+} versus H^+ ions, the disappearance of Pb from the media (Figure 2A) was slowest at pH 3 and the fastest at pH 5, with the maximum rates of adsorption being 2.3 x 10^{-3}, 5.6 x10^{-3} and 6.9 x 10^{-3} mmoles/min for pH 3, 4 and 5 respectively. By the end of the experiment, 33.6, 47.6 and 50.8% of the total Pb had been adsorbed from the media at pH 3, 4 and 5 respectively. At pH 7, the Pb speciation was still mainly as Pb^{2+} ions, but some $Pb(OH)^+$ was also present (Figure 2B). Nonetheless, the overall disappearance of total Pb from the media was 48.9% by end of the experiment, and similar to that at pH 5, albeit being initially a little slower at pH 7. The buoyancy of the aerogel during the batch adsorption experiments was also noted. During experiments where no Pb^{2+} was present in the media the aerogel continued to float just below the surface of the water for the entire 240 minutes. When Pb was present, the aerogel became denser than water and sank to the bottom of the test vessel within 3-6 minutes, an excellent 'indication' of Pb adsorption.

The effect of temperature on Pb adsorption by the aerogel was also explored at pH 5, with the adsorption being much faster at 22 °C than 4 °C (Figure 2C). Similar to experiments

at room temperature, the adsorption characteristics at 4 ºC fitted a two-parameter exponential decay ($r^2 > 0.99$). The maximum rate of disappearance of total Pb from the media was 6.9 x 10^{-3} and 2.8 x 10^{-3} mmoles/min at 22 and 4 ºC respectively, and with no significant difference of the amount of Pb remaining in the media at the higher temperature by the end of the experiment (Figure 2C).

The second series of experiments explored the disappearance of competing cations of different valencies from the media (no lead present). The adsorption of metal salts of Na^+, Ca^{2+}, Cu^{2+}, and La^{3+} are reported (Figure 2D). The competing cations were at equimolar starting concentrations to each other (all 0.48 mM) to enable comparisons between these ions, and with Pb in the first experiment at the same concentration. Only the water containing Cu^{2+} and La^{3+} (see supplementary Fig S3 for metal speciation plots) showed a steady decrease of the external total metal concentration over time, and with more adsorption of total Cu than La into the aerogel (Figure 2D). Both the Cu^{2+} and La^{3+} data were successfully fitted to a two parameter exponential decay curve ($r^2 > 0.99$). The maximum rate of adsorption for total Cu and La were 0.9 x 10^{-3} and 0.02 x 10^{-3} mmoles/min respectively, and with removal of 32 and 23% of the metal salt from the media respectively, over 240 minutes. In contrast to Cu, the Calcium nitrate adsorption experiment (Figure 2D) showed an initial increase of total calcium in the media, followed by some loss (presumed adsorption by the aerogel). This was partly expected as the synthesis of the aerogels included a 0.27 M $CaCl_2$ cross-linking step, and the initial rise in concentration likely reflects the release of residual Ca from the Ca-saturated aerogel followed by some re-adsorption as it equilibrates with the media. Notably, the curve for Na^+ was almost the mirror image of that for Ca^{2+}, with some initial total Na disappearance from the media and then some increase (desorption from the aerogel) and reaching equilibrium close to the starting concentration over the 240 minutes.

Figure 3 shows the maximum adsorption capacity of the GO aerogels for total Pb at different pH values, and in comparison with La and Cu at pH 5. For Pb, the adsorption capacity (q_e) is greatest at pH 5 with a value of 504 mg/g within 240 mins, compared to only 310 mg/g at pH 3. At pH 5, the adsorption capacity for Pb is considerably greater than that for either Cu or La, showing some specificity or preference for Pb adsorption.

The structure of the aerogel was also investigated by FTIR spectroscopy before and after exposure to Pb in water at pH 5 (Figure 4A). This showed a change in the functional groups as a result of the presumed Pb^{2+} binding to the aerogel after 240 minutes. The most significant shifts were at wavenumbers 3250, 2930, 1571, 1404, and 1292 cm^{-1} (Figure 4A).

For reference, a spectra is also shown for the dry aerogel (no hydration or Pb exposure). The wide adsorption peak at 3250 cm^{-1}, which is attributed O-H stretching (ν) vibration of the water molecules, increases in size on hydration of the aerogel as expected, but there is very little shift or attenuation of transmittance after 240 mins in water with/without Pb, indicating the aerogel is fully hydrated. Connected to this peak is the deformation at 2930 cm^{-1} which is also a stretching of the O-H vibration, but this is usually assigned to the -COOH group as both groups overlap. The latter data shows a slight shift in the peak and a reduction of intensity on Pb exposure and may indicate the acid residues were cross-linked by the Pb^{2+} cation. The stretching vibration of the C=C double bond, usually attributed to the aromatic ring in GO, shifts from 1593 cm^{-1} to 1571 cm^{-1} during the batch adsorption process, indicating a possible disruption to the ring structure or modification, furthermore, there is also a reduction in transmittance. Between the wavenumbers 1412 cm^{-1} and 1205 cm^{-1}, bending (δ) and deformation (β) of the O-H or C-OH groups on the aerogel is observed, which is attributed to the carboxylic acid group in non-stretching mode. This perturbation of the carboxylic acid group may be due to the increased mass attributed to Pb^{2+} binding to these functional groups. The C=O stretching bond usually attributed to the epoxy functional groups on the GO surface is clearly attenuated at 1292 cm^{-1}, and this is possibly due to the replacement of the oxygen by the Pb^{2+} cation. Similarly, the C-O usually attributed to the carboxyl group in the GO at 1055 cm^{-1} is attenuated due to possible deprotonation and the subsequent binding of the Pb^{2+} to the GO surface which is concurrent with the deformation of the peak at 2930 cm^{-1}. This method of analysis is purely qualitative and does not distinguish between the functional groups upon the GO or the acid residues of the alginate, but does confirm the overall modification within the aerogel structure.

Changes in the FTIR spectra might also be reflected in the ions lost from the aerogel on Pb exposure. Figure 4B shows the absolute amounts of the major ions that were present in the media before and after the Pb adsorption experiment at pH 5. Sodium and calcium are used in the synthesis of alginic acid and the cross-linking process; and both appear in the external media after the batch adsorption experiment with the aerogel and Pb^{2+} present. In an equivalent media without Pb and with just the aerogel, no other electrolytes appeared in the media; indicating that both Ca^{2+} and Na^{+} were released from the aerogel during the batch adsorption experiment. Notably, the sum of the absolute millimole quantity of Na^{+} and Ca^{2+} atoms combined that appear in the media is double the number of absolute Pb atoms that have disappeared from the media; suggesting that direct ion exchange is not the only mechanism driving the Pb^{2+} adsorption at pH 5. Figure 4C shows the absolute amount of Pb in the aerogel

recovered after *aqua regia* digestion of the samples at the end of the experiment. The amount of Pb found in the aerogel (Figure 4C) is almost the same as that lost from the media (about 0.1 mmoles absolute, Figure 4B); confirming that the Pb was adsorbed to the aerogel and not lost to the walls of the test vessel. The Na and Ca absolute millimole concentrations digested in *aqua regia* are not statistically different when comparing before and after the adsorption experiments.

The desorption kinetics of the aerogel are shown in Figure 5. These were determined firstly in weak HCl acid conditions at pH 5 and 3; then with much stronger acidic media (2% HCl and HNO_3). The rational to use HCl dropwise as the first weak acid desorption experiment brings the experiment in-line with pH adjustments throughout the adsorption experiments, replicating adsorption conditions, to understand the reversibility of total Pb mobility in almost identical conditions. The stronger acid conditions are an attempt to force any remaining Pb from within the aerogel into the surrounding solution for complete desorption. The use of HNO_3 as an alternative strong acid wash was to assess the potential effect of a strong oxidiser upon the structure. In weak acid conditions, there was negligible desorption of Pb at pH 5, but at pH 3 some Pb appeared in the external media (Figure 5A) and this was approximately returning 50% of the total Pb typically adsorbed by the aerogel after 240 mins. Stronger acids, 2% HNO_3 and 2% HCl returned the total Pb concentration back into media at a faster rate and at a much higher final concentration; recovering 99% the Pb within six minutes, regardless of the acid used (Figure 5B). Upon visual observation after desorption in 2% HCl the overall structural integrity of the aerogel had become more gelatinous in nature, while still retaining its structure, indicating that the cross-linking or bonds in the aerogel had changed in a qualitative manner, this was not as evident for 2% HNO_3.

4. Discussion

This study demonstrates that a biopolymer aerogel synthesised from GO and alginate can adsorb over 500 mg/g of Pb within 240 minutes; on average a tenfold improvement on previous reports using naturally derived activated carbon (Wang et al., 2010). The Pb adsorption is pH-dependent with the maximum adsorption at pH 5, and the Pb is partly taken up in exchange for Ca^{2+} and Na^{+} ions from the aerogel. The aerogel adsorbs Pb more strongly than other metals such as Cu^{2+} or La^{3+}, and can be washed in for a few minutes in 2% HNO_3 or HCl to reclaim the metal ions. The aerogel is mechanically robust, withstanding magnetic

stirring during batch adsorption and is acid resistant maintaining its structure in 2% HNO_3 for over a 3 month period.

The innovations of this novel approach to lead adsorption is the use of an aerogel structure which maintains a large specific surface area for active binding events. The robust macroporous network exhibits non-limiting diffusion kinetics during the early stages of adsorption and is latterly supported by the ion-exchange cascade mechanism, possibly involving proton tunnelling, resulting in an adsorption capacity above and beyond other adsorbents per unit weight with a similar structure. The significance of such material is the ability to adsorb high concentrations of the contaminants within a short period of time and conversely remove low concentrations of contaminants over longer periods without becoming saturated, reducing replacement costs and increasing efficiency compared with existing adsorption materials. In practical terms the aerogel would be housed within a syringe style filter structure providing quick and simply replacement for regeneration and preventing unintended release of the GO.

4.1. Characterisation and structure of the aerogel

Aerogels produced using similar methodologies are comparable to the aerogels synthesised in this study (Mi et al., 2012). The pore sizes previously reported range from 50 – 200 micrometres and in comparison our aerogels range from 50-150 micrometres with a non-specified morphology. Figure 1E – H gives an overview of the structure illustrating uniform pore distribution, magnifying a single pore for further clarity. A lattice size of (nm-µm) allows the easy diffusion of ions (pm), the aerogels can tolerate saline (as Na and Ca) as well as acidic conditions, remain robust and durable even after washing in 2% HNO_3 and are fabricated without impurities (Figure 1D).

4.2. Effects of pH, external cations and temperature on Pb adsorption

The aerogel structure provides a polyanionic matrix of fixed negative charges via the carboxyl groups on the organic acid moieties of the alginate (Figure 6). Since the aerogel was prepared using 4% $CaCl_2$ to enable cross-linking of the alginate, the carboxyl residues therein will be charge screened by mainly Ca^{2+} ions, but also by any Na^{+} remaining from the natural alginate. From the viewpoint of ion exchange theory, the L-guluronic acid (G-block) and D-mannuronic acid (M-block) moieties within the alginate have dissociation constants for acid

(pKa values) of 3.38 and 3.65, respectively (Ching et al., 2017). So, these moieties will have an increasingly strong net negative charge at pH 4 and above, but can become saturated with H^+ ions at pH 3 where the net negative charge is partially lost due to charge screening. Any adsorption of Pb into the aerogel by ion exchange would therefore be pH-dependent, as observed (Figure 2A). Metal ion binding to polyanionic matrices will also depend on the mobility of the metal ion relative to H^+ (the fastest diffusing ion in solution), the valency or charge density of the metal, and the concentration of each competing ion (Handy and Eddy, 2004). For the latter, the Pb^{2+} ion activity is also dependent on the metal speciation in solution, and below pH 5 especially, the Pb^{2+} ion dominates, but even at pH 7 there is a good supply of Pb^{2+} (Figure 2B). Consequently, in the experimental conditions here (Figure 2A) Pb^{2+} ions will be attracted to the fixed negative charge of the aerogel at pH 4 or higher (i.e., above the pKa values), but at pH 3 the H^+ is more effective at competing with Pb^{2+} and so the apparent adsorption slows with a lower capacity (Figure 2A). The Pb adsorption at pH 5 is better than pH 7, simply because the Pb speciation provides 20% more Pb^{2+} ions at pH 5 when the supply of H^+ has changed by only 10 µM.

If the aerogel is simply behaving like an ion exchange resin, it would be expected that: (i) milliequivalent concentrations of ions will be lost from the aerogel (i.e., the Ca^{2+}, Na^+, and any H^+) in exchange for the Pb; and (ii) that the aerogel will selectively adsorb metal ions according to their valency or charge density. For the former aspect, in our experimental conditions, Pb exposure was displacing Ca^{2+} and Na^+ ions into the media (Figure 4); but it was not equimolar; with twice as much Ca^{2+} and Na^+ released than Pb taken up, suggesting mechanisms in addition to simple ion exchange are driving the high performance of the aerogel. Secondly, for metal adsorption by ion exchange alone, the metals La^{3+}, Pb^{2+} and Cu^{2+} should show adsorption capacities in accordance to their charge density, calculated from the hydrated ionic radii and valency. The hydrated ionic radii (Stokes radius) are 3.96, 2.83, 3.25 Å for La^{3+}, Pb^{2+} and Cu^{2+} respectively (Nightingale Jr, 1959), with calculated charge densities of 0.757, 0.706 and 0.615 Cm^{-3} respectively. Thus, ion exchange theory would predict the adsorption capacity in the order: $La^{3+}>Pb^{2+}>Cu^{2+}$. However, despite using equimolar concentrations of each metal (100 mg/l – 0.48 mM) and the species of the free metal ion not being limiting at pH 5 (Figure 2B, Figure S3), Figure 2C shows that the total Cu is removed from the media faster than La, and with much more adsorption of Pb than the other metals (compare Figures 2A and 2C). The maximum adsorption capacity ranks the metals in this order at pH 5: $Pb^{2+}>La^{3+}>Cu^{2+}$. Again, suggesting the behaviour of the aerogel is not explained by simple ion exchange and charge density alone.

Alternatively, the diffusion path through the lattice of the aerogel may be the limiting factor in the removal rate of metal from the external media and in the overall binding capacity. The diffusion coefficients for each metal were calculated from equation (4) and the values were 7.635×10^{-10}, 6.645×10^{-10} and 5.454×10^{-10} $m^2\ s^{-1}$ for Pb^{2+}, Cu^{2+} and La^{3+} respectively and while these are in the same order as the maximum adsorption capacity (Figure 3); the adsorption capacity for Pb is still twice that of the other metals suggesting that factors other than the diffusion coefficient are enabling the high performance of Pb adsorption by the aerogel. The diffusion coefficient is also partly dependent on the ambient temperature, and using equation (4) the diffusion coefficient for Pb^{2+} in the media was 7.170×10^{-10} $m^2\ s^{-1}$ at 4 ^oC compared to 7.635×10^{-10} $m^2\ s^{-1}$ at 22 °C (i.e., only a 6% difference). In contrast, the maximum rates of Pb disappearance from the media taken from the initial slopes (Figure 2C) when diffusion should not be limiting were 2.8×10^{-3} and 6.9×10^{-3} mmoles/min at the two temperatures; equating to an 86% difference that is far beyond any expected temperature effect on diffusion. Together these observations suggests that diffusion and traditional ion exchange phenomena expected in the alginate only partly explains the performance of the aerogel.

4.3. Kinetic models for Pb uptake into the aerogel

The data in Figure 2 were also fitted to pseudo first order, pseudo second order and intraparticle diffusion kinetics models for Pb^{2+} adsorption respectively (see the supplementary data). While there was a little variation in the initial data points in the first few minutes of the adsorption kinetics, overall both the first order (Figure S4A) and second order kinetic (Figure S4B) models gave good fits (r^2 values from 0.93 – 0.99 and 0.8 – 0.98 respectively). However, adsorption of Pb at pH 5, where the maximum adsorption capacity occurs, best fitted the second order, rather than the first order, kinetic model with an r^2 value of 0.98. Also supporting this hypothesis is the calculated q_e values from the kinetic model linear equations, compared to the experimental value of q_e, it is evident from Table S1 that the pseudo second order model gives the closest correlation between theory and experiment. This confirms the notion of at least two steps in Pb^{2+} adsorption, i.e., diffusion into the aerogel and then ion binding events inside the lattice structure (as discussed above). Notably, at 4° C, the second order model was a poorer fit (r^2 = 0.34, Fig S6B), and consistent with the notion of another mechanism being involved in Pb adsorption (see below).

The intraparticle diffusion model explores the idea that binding of Pb^{2+} (any metal) to the core of the aerogel is diffusion limited and that any initial binding of Pb^{2+} to the periphery

of the aerogel lattice will result in a Pb-saturated boundary layer while parts of the core remain unoccupied by Pb atoms. This would require three compartments (the outside, the periphery of the aerogel and its core) and indeed multiple linear regressions reveal three components to the absorption curves (e.g., Figure S4D for Pb^{2+} at different pH). Surprisingly, this was not the case for La^{3+} and Cu^{2+} (Figure S5D); with the single regression of the intraparticle diffusion model giving arguably the best r^2 values of 0.96 and 0.98 for Cu^{2+} and La^{3+} respectively. An alternative interpretation is that the three compartments in the model are the outside, the alginate of the aerogel and the GO; but this does not fit the data. For example, in traditional chemistry, there is no reason for Pb^{2+} to distinguish between a hydroxyl residue on GO compared to that on the alginate moieties, so the alginate and GO are seen as one pool with respect to kinetics (but see below on the exception of Pi stacking (π-π stacking) in GO). Also, at pH 3, the multiple regressions for the intraparticle model show only two compartments, supporting the idea that all the internal ligands are occupied at pH 3 (i.e., exceeding the pKa), and so only the outside/boundary layer and diffusion inside the aerogel remain.

4.4. Graphene oxide and enhanced performance of the aerogel for the adsorption of lead

One possibility to consider is that the addition of GO to the structure of the aerogel had enhanced its performance beyond that expected of diffusion and ion exchange by the alginate alone which makes up the bulk of the material. Figure 6 shows the expected arrangement and bonding of GO with the moieties of the alginate. The Pb^{2+} ions can displace Ca^{2+} from the carboxyl residues of the organic moieties of the alginate (discussed above), but there is also the possibility of Pb forming hydroxyl complexes by solvation with fixed anions (Scott, 1989), such as the abundant hydroxyl groups on the graphene oxide. Indeed, the carboxyl and hydroxyl residues on the edges of the GO sheets, and the epoxide and hydroxyl groups on the basal planes of GO sheets are known to bind Pb^{2+} according to the following reaction sequences (Peng et al., 2016).

$$-COOH + Pb^{2+} + -OH \rightarrow -COOPbO^{-} + 2H^{+} \quad (5)$$

$$-COOH + Pb^{2+} \rightarrow -COOPb^{+} + H^{+} \quad (6)$$

$$-OH + Pb^{2+} \rightarrow -OPb^{+} + H^{+} \quad (7)$$

$$-2COOH + Pb^{2+} \rightarrow -COOPbOOC- + 2H^{+} \quad (8)$$

$$-2OH + Pb^{2+} \rightarrow -OPbO^{-} + 2H^{+} \quad (9)$$

The FTIR measurements (Figure 4A) also support these reaction sequences with notable modifications of the spectra at wavenumbers 3250, 2930, 1571, 1404, and 1292 cm^{-1} (see results section), which documents the changes to the carboxyl and hydroxyl functional groups as seen in equations 4 -7. Moreover, given the abundance of such residues on the GO, the equilibrium adsorption capacity for Pb on pure GO is around 700 mg/g with Pb additions of 20 mg/l or more (Peng et al., 2016). Thus, despite the 1:13 ratio of GO:alginate in the aerogels here, the GO would still likely adsorb a significant fraction of the Pb. Notably with Cu, which has a very similar speciation chemistry to Pb in water with similar pH, and Cu^{2+} dominates below pH 5, but unlike Pb^{2+}, Cu^{2+} seems to form coordination groups only with oxygen atoms on the GO; and consequently the GO adsorbs much less Cu with maximum absorption capacities around 50 mg/g with 10 mg/l of Cu (Wang et al., 2018). In contrast to both Pb and Cu, additions of $LaCl_3$ to dispersions of GO causes coagulation of the GO and disorganisation of the graphene structure (Chen et al., 2017b), perhaps partly explaining the limited adsorption capacity in the aerogels here (Figure 3). The enhanced performance with Pb compared to Cu or La, might also be explained by the similar valency and hydrated ionic radius of Pb^{2+} (2.83 Å) with Ca^{2+} (3.1 Å); indicating that Pb^{2+} will preferentially compete with the Ca^{2+} for binding sites on the aerogel. Any displaced Ca^{2+} might then also displace Na^{+} from residues in the aerogel in a cascading effect (hydrated ionic radius of Na^{+}, 1.84 Å), resulting in the net Ca^{2+} and Na^{+} loss to the external media. Indeed, this competition between Pb^{2+} and Ca^{2+} for biological ligands is very well established [e.g., the Pb in the Biotic Ligand Model (BLM), Macdonald et al. (2002)] (Macdonald et al., 2002).

The proposed spatial arrangement of the GO in the aerogel (Figure 6) may have also contributed to the enhanced performance with Pb^{2+} compared to Cu^{2+} or La^{3+}. Graphene oxide is known to attract to polyanionic surfaces, such as those in the moieties of aerogels by π-π stacking along with some hydrogen bonding (Yao et al., 2017). The interlayer spacing of a pure GO membrane is approximately 11.7 Å, as reported by Li et al. (2018), suggesting sufficient space for all hydrated cations used in this study to intercalate between the layers and coordinate with the epoxy groups on the GO platelets (Li et al., 2018). However, it is unknown how the layers of alginate effect this interlayer spacing, perhaps decreasing it thus slowing the mobility of larger ions like La^{3+}. Any hydrogen-metal bonding in this space with Pb^{2+} will also be much stronger than that for Cu^{2+} (Łosiewicz et al., 2015). Also, the effect of decreasing temperature on Pb^{2+} adsorption rates cannot readily be explained by a simple diffusion model (discussed above), and with multiple Pb^{2+} atoms of 2.83 Å in a space of only 11.7 Å, or less, the possibility of H^{+} tunnelling, which shows temperature independence (Kohen and Klinman, 1999), cannot

be excluded. In narrow atomic spaces, H^+ diffusion is much higher in the presence of Pb than other metal atoms (Hartmann, 1991). Consequently, this quantum tunnelling effect could manifest as much higher Pb adsorption compared to other metals at acidic pH, as observed in Figure 3. The GO-enhanced Pb absorption properties of the aerogels needs further investigation.

4.5. Desorption of lead and utility of the aerogel

Desorption of the Pb^{2+} from the aerogel using ultrapure water in acid conditions is arguably the reverse of the ion exchange and diffusion processes discussed above. At pH 5 with weak acid there was no desorption of total Pb into the media, but at pH 3, H^+ concentration is in excess, causing Pb to appear in the external media (Figure 5A). This observation is readily explained by protonating the anionic residues in the aerogel in exchange for the Pb^{2+} at low pH, followed by diffusion of the Pb^{2+} down the concentration gradient and into the external medium. In these conditions with weak HCl, the aerogel remained intact, but not all of the Pb was washed out of the aerogel. It was not the purpose of the study to explore the re-use and regeneration of the aerogel, but the opportunity was taken to determine if a stronger acid could wash out the accumulated Pb more quickly (Figure 5B). With either 2% HNO_3 or HCl, the majority of the Pb was recovered within a few minutes (Figure 5B); suggesting that an acid wash would be a practical way of recovering any metal and regenerating the aerogel. However, very strong HCl caused the aerogel to become soft and gelatinous (although still intact). This change in texture is likely because the moieties in the alginate had become partially delinked as a result of removing the Pb^{2+} cations, and an addition soak in $CaCl_2$ might therefore restore the rigidity of the aerogel.

5. Conclusion

A GO alginate aerogel was fabricated for the removal of toxic metals from water. The macroscopic pore structure allows for a high adsorption rate and a binding capacity for over 500 mg/g of Pb^{2+} cations within 240 minutes. The aerogel operates at a range of pH values and is therefore ideally situated to cope with varying water quality. It also shows selectivity for Pb^{2+} cations compared to other metals with the same valency and is about ten times more efficient than standard activate carbon. The primary adsorption mechanisms are diffusion and then ion exchange, but the intraparticle diffusion model suggests at least three compartments,

and the possibility of GO enhancing Pb^{2+} binding via π-π stacking and other mechanisms. Further investigations are needed to elucidate any such phenomena. Lead can be desorbed easily from the aerogel by acid washing, thus allowing recovery of any metal and the potential to reuse the aerogel.

Conflict of interests

The authors declare no conflicts of interests.

Acknowledgments

This project was funded by the University of Plymouth, project code, GD105237 - 105. Technical support from Mr Nick Fry for Clean Room methods, Mr Andrew Atfield and Dr William Vevers for fabrication methodologies, Dr Rob Clough and Dr Andrew Fisher for ICP-OES metal analysis techniques and lastly Miss Jane Ankerman and Ms Alex Fraser for freeze drying methods is acknowledged.

References

Balli, N., Leghouchi, E., 2018. Assessment of lead and cadmium in groundwater sources used for drinking purposes in Jijel (Northeastern Algeria). GLOBAL NEST JOURNAL. 20**,** 417-423.

Barbosa Jr, F., et al., 2005. A critical review of biomarkers used for monitoring human exposure to lead: advantages, limitations, and future needs. Environmental health perspectives. 113**,** 1669-1674.

Boskabady, M., et al., 2018. The effect of environmental lead exposure on human health and the contribution of inflammatory mechanisms, a review. Environment international. 120**,** 404-420.

Canfield, R. L., et al., 2003. Intellectual impairment in children with blood lead concentrations below 10 μg per deciliter. New England journal of medicine. 348**,** 1517-1526.

Chen, L., et al., 2017a. High performance agar/graphene oxide composite aerogel for methylene blue removal. Carbohydrate polymers. 155**,** 345-353.

Chen, X., et al., 2017b. La (III) coagulated graphene oxide for phosphate binding: mechanism and behaviour. International Journal of Environmental Studies. 74**,** 586-602.

Ching, S. H., et al., 2017. Alginate gel particles–A review of production techniques and physical properties. Critical reviews in food science and nutrition. 57**,** 1133-1152.

Claramunt, S., et al., 2015. The importance of interbands on the interpretation of the Raman spectrum of graphene oxide. The Journal of Physical Chemistry C. 119**,** 10123-10129.

Commission, E., 1998. Council Directive 98/83/EC of 3 November 1998 on the quality of water intended for human consumption. Official journal of the European communities. 41**,** 32-54.

Di Baldassarre, G., et al., 2018. Water shortages worsened by reservoir effects. Nature Sustainability. 1, 617-622.
Douay, F., et al., 2013. Assessment of potential health risk for inhabitants living near a former lead smelter. Part 1: metal concentrations in soils, agricultural crops, and homegrown vegetables. Environmental monitoring and assessment. 185, 3665-3680.
Edwards, M., 2013. Fetal death and reduced birth rates associated with exposure to lead-contaminated drinking water. Environmental science & technology. 48, 739-746.
Fang, Q., Chen, B., 2014. Self-assembly of graphene oxide aerogels by layered double hydroxides cross-linking and their application in water purification. Journal of Materials Chemistry A. 2, 8941-8951.
Handy, R. D., Eddy, F. B., 2004. Transport of solutes across biological membranes in eukaryotes: An environmental perspective. IUPAC SERIES ON ANALYTICAL AND PHYSICAL CHEMISTRY OF ENVIRONMENTAL SYSTEMS. 9, 337-356.
Hartmann, O., 1991. New results on diffusion in fcc metals. Hyperfine Interactions. 64, 641-648.
Homayouni, A., et al., 2007. Effect of lecithin and calcium chloride solution on the microencapsulation process yield of calcium alginate beads.
Kohen, A., Klinman, J. P., 1999. Hydrogen tunneling in biology. Chemistry & biology. 6, R191-R198.
Kundu, D. K., et al., 2018. Experimenting with a novel technology for provision of safe drinking water in rural Bangladesh: The case of sub-surface arsenic removal (SAR). Technology in Society.
Li, W., et al., 2018. Controlling interlayer spacing of graphene oxide membranes by external pressure regulation. Acs Nano. 12, 9309-9317.
Liu, J., et al., 2016. 3D graphene/δ-MnO 2 aerogels for highly efficient and reversible removal of heavy metal ions. Journal of Materials Chemistry A. 4, 1970-1979.
Łosiewicz, B., et al., Intermetallic Compounds as Catalysts in the Reaction of Electroevolution/Absorption of Hydrogen. Solid State Phenomena, Vol. 228. Trans Tech Publ, 2015, pp. 16-22.
Lowry, J. A., 2010. Oral chelation therapy for patients with lead poisoning. Am Acad Pediatr. 116, 1036-1046.
Macdonald, A., et al., 2002. A lead–gill binding model to predict acute lead toxicity to rainbow trout (Oncorhynchus mykiss). Comparative Biochemistry and Physiology Part C: Toxicology & Pharmacology. 133, 227-242.
Maleki, H., 2016. Recent advances in aerogels for environmental remediation applications: a review. Chemical Engineering Journal. 300, 98-118.
Marcano, D. C., et al., 2010. Improved synthesis of graphene oxide. ACS nano. 4, 4806-4814.
Meena, A. K., et al., 2005. Removal of heavy metal ions from aqueous solutions using carbon aerogel as an adsorbent. Journal of hazardous materials. 122, 161-170.
Mekonnen, M. M., Hoekstra, A. Y., 2016. Four billion people facing severe water scarcity. Science advances. 2, e1500323.
Mi, X., et al., 2012. Preparation of graphene oxide aerogel and its adsorption for Cu2+ ions. Carbon. 50, 4856-4864.
Motahari, S., et al., 2016. Absorption of heavy metals using resorcinol formaldehyde aerogel modified with amine groups. Desalination and Water Treatment. 57, 16886-16897.
Nightingale Jr, E., 1959. Phenomenological theory of ion solvation. Effective radii of hydrated ions. The Journal of Physical Chemistry. 63, 1381-1387.
Pan, L., et al., 2018. Efficient removal of lead, copper and cadmium ions from water by a porous calcium alginate/graphene oxide composite aerogel. Nanomaterials. 8, 957.
Peng, W., et al., 2016. Comparison of Pb (II) adsorption onto graphene oxide prepared from natural graphites: Diagramming the Pb (II) adsorption sites. Applied Surface Science. 364, 620-627.
Qu, X., et al., 2013. Applications of nanotechnology in water and wastewater treatment. Water research. 47, 3931-3946.

Sankhla, M. S., et al., 2016. Heavy metals contamination in water and their hazardous effect on human health-a review. Int. J. Curr. Microbiol. App. Sci (2016). 5**,** 759-766.
Scott, J. E., Ion binding: patterns of'affinity'depending on types of acid groups. Symposia of the Society for Experimental Biology, Vol. 43, 1989, pp. 111-115.
Stauber, J., et al., 1994. Percutaneous absorption of inorganic lead compounds. Science of the total environment. 145**,** 55-70.
Talukder, M. R. R., et al., 2016. The effect of drinking water salinity on blood pressure in young adults of coastal Bangladesh. Environmental Pollution. 214**,** 248-254.
Van de Wiele, T. R., et al., 2007. Comparison of five in vitro digestion models to in vivo experimental results: lead bioaccessibility in the human gastrointestinal tract. Journal of Environmental Science and Health Part A. 42**,** 1203-1211.
Wang, H., et al., 2018. Removal of copper ions by few-layered graphene oxide nanosheets from aqueous solutions: external influences and adsorption mechanisms. Journal of Chemical Technology & Biotechnology. 93**,** 2447-2455.
Wang, L., et al., 2010. Adsorption of Pb (II) on activated carbon prepared from Polygonum orientale Linn.: kinetics, isotherms, pH, and ionic strength studies. Bioresource technology. 101**,** 5808-5814.
Wang, M., et al., 2019. Highly efficient removal of copper ions from water by using a novel alginate-polyethyleneimine hybrid aerogel. International journal of biological macromolecules. 138**,** 1079-1086.
WHO, 2011. Guidelines for drinking-water quality. WHO chronicle. 38**,** 104-8.
Yao, Q., et al., 2017. 3D assembly based on 2D structure of cellulose nanofibril/graphene oxide hybrid aerogel for adsorptive removal of antibiotics in water. Scientific Reports. 7**,** 45914.
Zhang, H., 2002. Regeneration of exhausted activated carbon by electrochemical method. Chemical Engineering Journal. 85**,** 81-85.
Zuo, L., et al., 2015. Polymer/carbon-based hybrid aerogels: preparation, properties and applications. Materials. 8**,** 6806-6848.

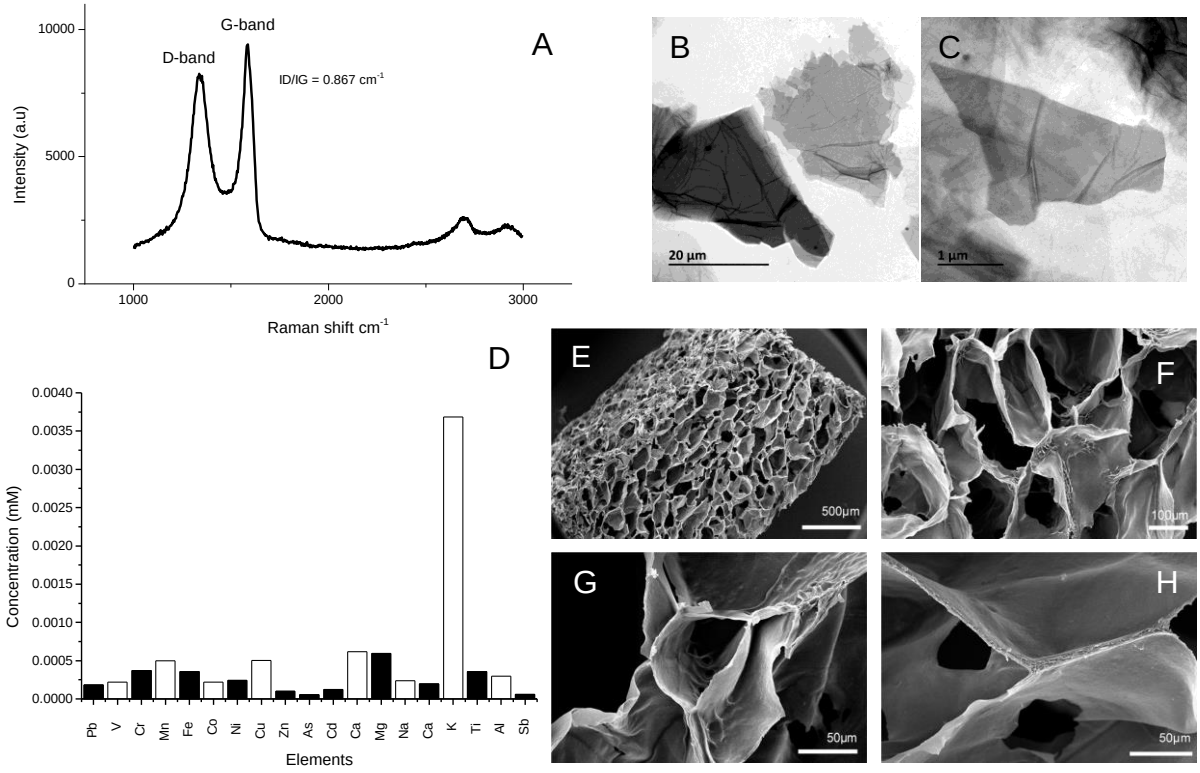

Figure 1. Raman spectra of pure GO, peak ratio ID/IG = 0.867 cm^{-1} (A), TEM of pure GO platelets, bi-layer and multilayer, (B-C), ICP-OES analysis of pure GO purity after synthesis (D), SEM of GO aerogels, overview of monolith (E), image of larger pores ~150 µm (F), image of smaller pores ~50 µm, meeting node of pores revealing a 5 – 10 µm pore wall thickness (H).

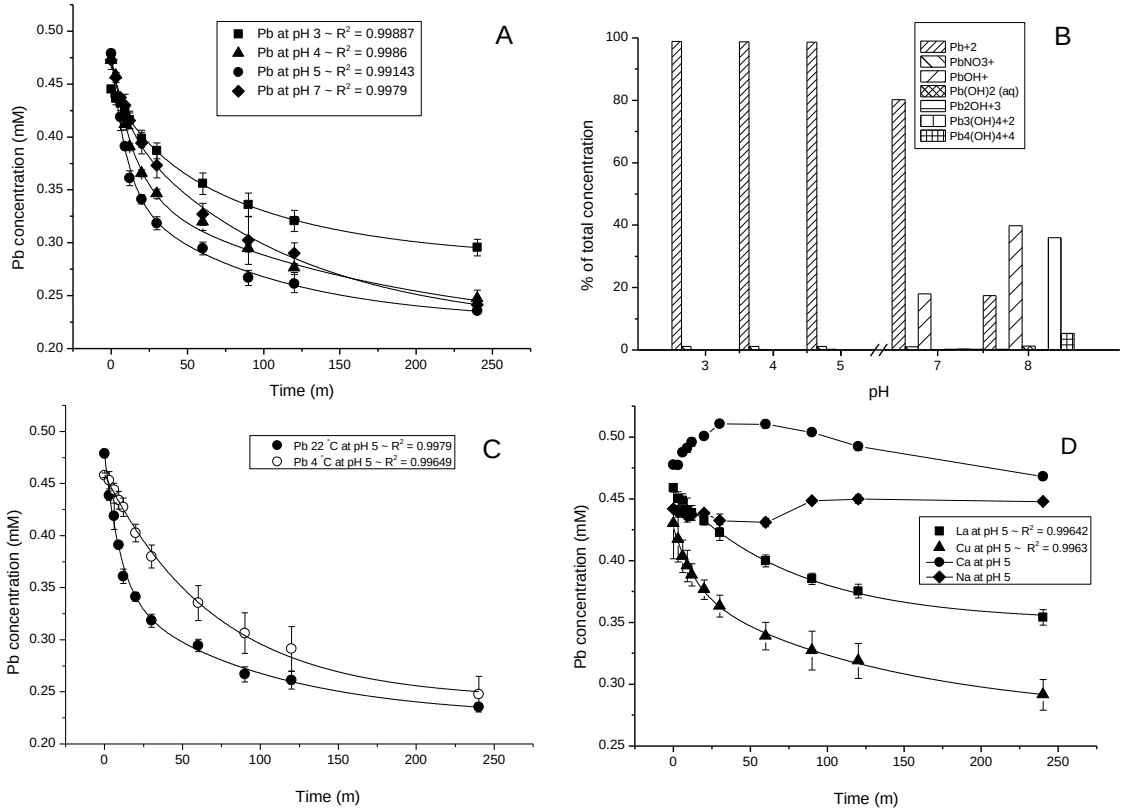

Figure 2. Lead adsorption into the aerogels as measured by the disappearance of total Pb from the external media at varying pH values at initial concentration of 0.48 mM (100mg/l) (A), the speciation of lead in the ultrapure water calculated using visual MINTEQ 3.1 (B), lead adsorption at two temperatures, 22 and 4 °C both at pH 5 in ultrapure water (C), the adsorption of monovalent, divalent and trivalent ions to GO aerogel using salt solutions of Na^{+}, Ca^{2+}, Cu^{2+} and La^{3+} at pH 5 and (D). All data are means with ±SD, n = 4, ANOVA test on panel A at 240 mins $P < 0.05$. Decay curves were fitted with a two parameter exponential decay with r^2 value for all > 0.99 (see supplementary information for kinetic models and figure S2 for ANOVA box plot chart).

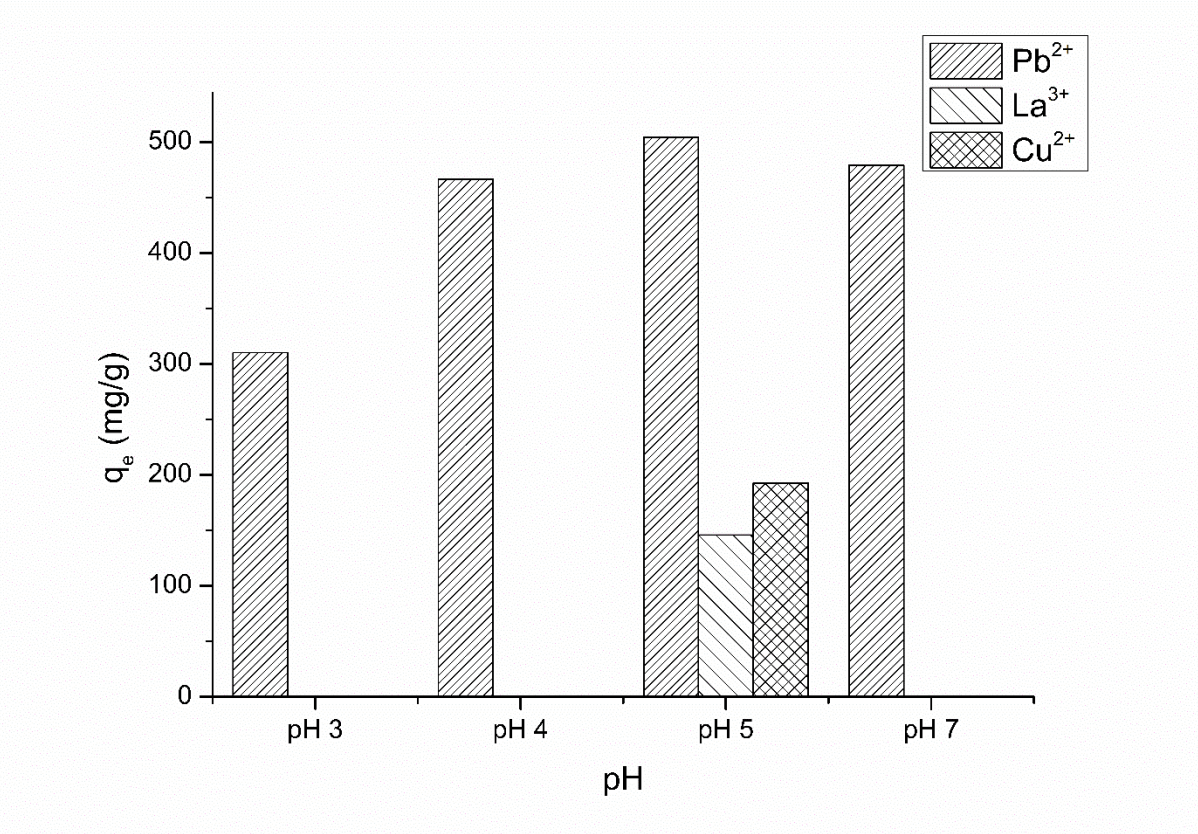

Figure 3. Maximum adsorption capacity of GO aerogel in mg/g for Pb^{2+} from pH 3 – 7 and a comparison of La^{3+} and Cu^{2+} at pH 5 demonstrating selectivity for Pb. Data for Pb^{2+} are 310.2, 466.5, 504.1 and 479.1 mg/g for pH 3, 4, 5 and 7 respectively and the data for La^{3+} and Cu^{2+} are 145.7 and 192.6 mg/g respectively.

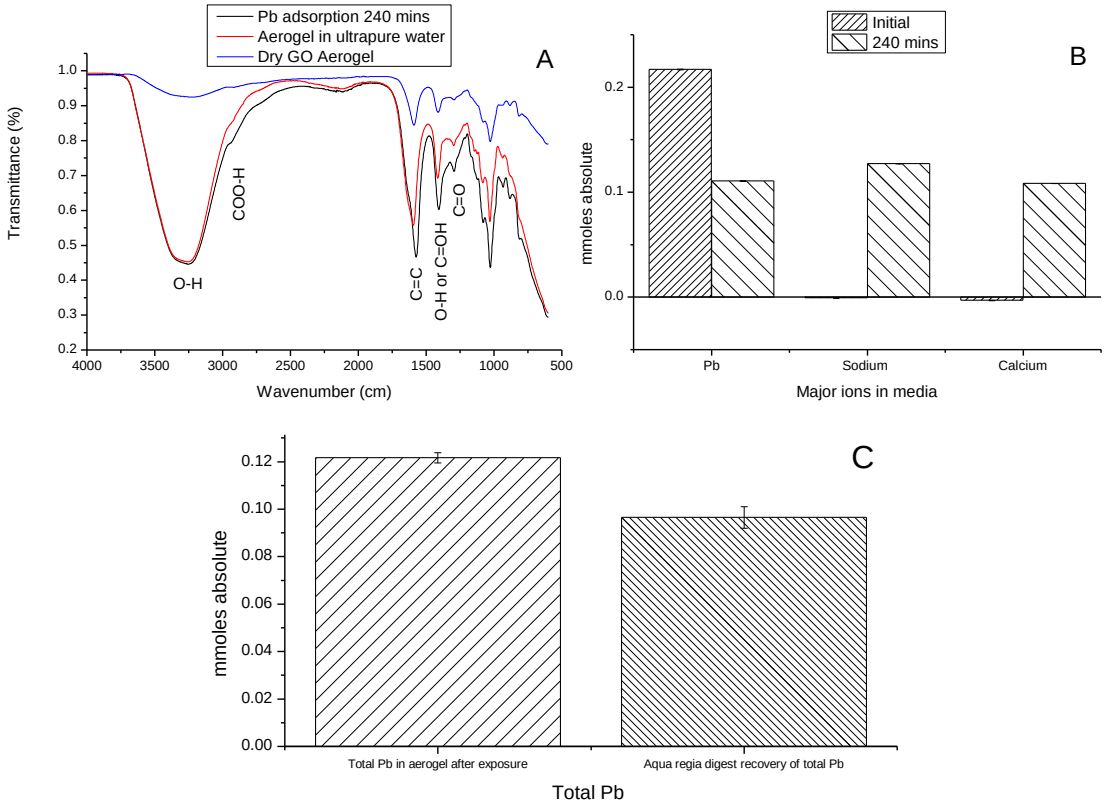

Figure 4. FTIR of hydrated GO aerogel before adsorption experiment in ultrapure water and after Pb adsorption experiment with a dry GO aerogel as a reference (A), ion absolute ion concentrations in the external media before and after Pb exposure at pH 5 in millimoles absolute (B), aqua regia digest recovery of total Pb in millimoles absolute from the aerogel after exposure during adsorption experiment (using data from caption B), representing 82% recovery (C). All data are means with ±SD, n = 4, except panel A which is mean data, n = 3.

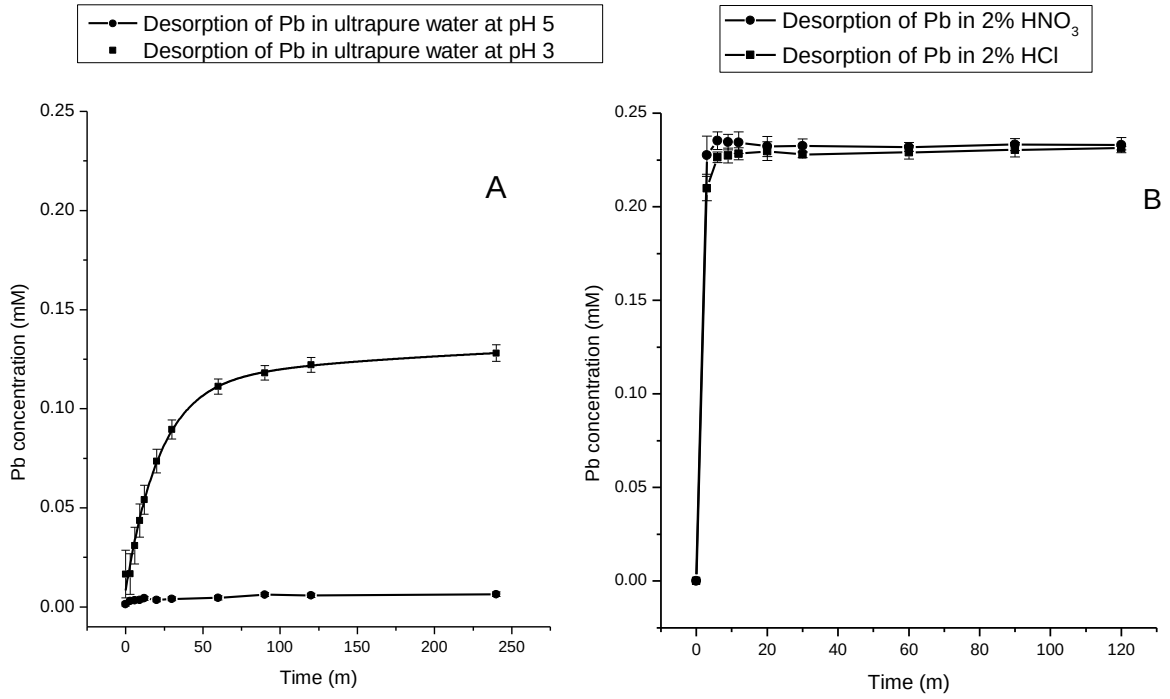

Figure 5. Desorption of Pb loaded GO aerogel in weak acidic conditions, at pH 5 and pH 3, curve at pH 3 fitted with a second order exponential growth curve with an R^2 value > 0.99, line omitted in legend (A), Desorption of Pb loaded aerogel in stronger acidic conditions, 2% HNO_3 and 2% HCl (B). All data are means with ±SD, n = 4.

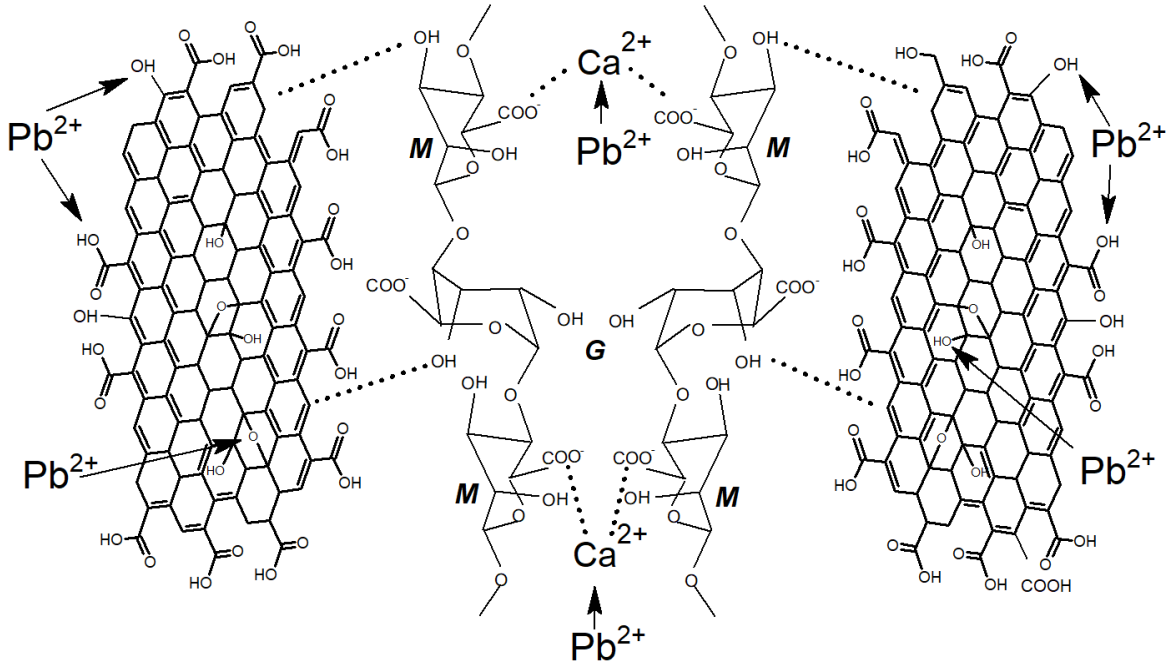

Figure 6. Potential binding sites for Pb within the aerogel. The primary route is the ion exchange of the Pb^{2+} ions and Ca^{2+} ions from the carboxyl residues of the organic alginate moieties. Pb^{2+} ions can also form hydroxyl complexes with fixed anions on the graphene oxide as well as the carboxyl residues on the edges of the GO sheets and the epoxide groups on the basal planes resulting in multiple site for the binding the Pb^{2+} ions.